Received: 22 January 2020 | Revised: 29 April 2020 | Accepted: 29 May 2020

DOI: 10.1111/jace.17328

ORIGINAL ARTICLE

Journal of the American Ceramic Society

Resistance of pure and mixed rare earth silicates against calcium-magnesium-aluminosilicate (CMAS): A comparative study

Markus Wolf[1] | **Daniel Emil Mack**[1] | **Olivier Guillon**[1,2] | **Robert Vaßen**[1]

[1]Institute of Energy and Climate Research, Materials Synthesis and Processing (IEK-1), Forschungszentrum Jülich GmbH, Jülich, Germany

[2]Jülich Aachen Research Alliance: JARA-Energy, Jülich, Germany

Correspondence
Markus Wolf, Institute of Energy and Climate Research, Materials Synthesis and Processing (IEK-1), Forschungszentrum Jülich GmbH, Jülich, Germany.
Email: m.wolf@fz-juelich.de

FUNDING INFORMATION
The authors acknowledge financial support from MTU Aero Engines AG under contract Z0609.21.18.

Abstract

Rare earth silicate environmental barrier coatings (EBCs) are state of the art for protecting SiC ceramic matrix composites (CMCs) against corrosive media. The interaction of four pure rare earth silicate EBC materials Yb_2SiO_5, $Yb_2Si_2O_7$, Y_2SiO_5, $Y_2Si_2O_7$ and three ytterbium silicate mixtures with molten calcium-magnesium-aluminosilicate (CMAS) were studied at high temperature (1400°C). The samples were characterized by SEM and XRD in order to evaluate the recession of the different materials after a reaction time of 8 hours. Additionally, the coefficient of thermal expansion (CTE) was determined to evaluate the suitability of Yb silicate mixtures as EBC materials for SiC CMCs. Results show that monosilicates exhibit a lower recession in contact with CMAS than their disilicate counterparts. The recession of the ytterbium silicates is far lower than the recession of the yttrium silicates under CMAS attack. Investigation of the ytterbium silicate mixtures exposes their superior resistance to CMAS, which is even higher than the resistance of the pure monosilicate. Also their decreased CTE suggests they will display better performance than the pure monosilicate.

KEYWORDS

apatite, ceramic matrix composites, CMAS, corrosion/corrosion resistance, environmental barrier coatings (EBCs), thermal expansion

1 | INTRODUCTION

Due to an increase in the overall operating temperature of the hot section, aircraft turbine engines can achieve higher fuel efficiencies while simultaneously reducing environmentally harmful byproducts. However, the operating temperature of gas turbines using currently available nickel-based alloys can only be further increased by employing improved cooling techniques and advanced thermal barrier coatings (TBCs). Unfortunately, the use of cooling air reduces the efficiency of the hot section in turbine systems. Current research, therefore, focuses on new material concepts such as silicon-carbide-based ceramic matrix composites (CMCs), which require reduced cooling because of their higher temperature capability.[1–4] In the field of high-temperature applications, SiC CMCs show improved thermomechanical stability and superior mechanical properties, for example, creep resistance, in comparison to nickel-based alloys. Furthermore, they exhibit lower density, which results in component weight reduction.[5–7] In oxidizing environments, a passivating layer of SiO_2 forms via reaction (1) on the silicon-based CMC, which reduces oxidation of the underlying material. However, these materials suffer from rapid recession when the protective character of SiO_2 vanishes in a fast-flowing,

high-temperature water vapor atmosphere, since SiO_2 continues reacting to $Si(OH)_4$). This reaction product becomes volatilized thus resulting in severe material loss.[8–10]

In order to suppress corrosion, environmental barrier coatings (EBCs) have been developed to prevent the degradation of SiC/SiC CMCs in oxidizing and water vapor. In contrast to TBCs, EBCs must be dense to inhibit permeation of water vapor and oxygen to the substrate. In addition to high resistance to degradation by water vapor, EBC materials need high phase and thermal stability, chemical compatibility with SiC, and a high melting point for applications above 1200°C. Furthermore, the difference of the coefficient of thermal expansion (CTE) between the EBC and SiC/SiC must be as low as possible to avoid thermal stresses in the coating during thermal cycling, which can be a possible cause of failure of the protective system.[11–15]

Recent studies on advanced EBCs have focused on rare earth (RE) silicates. Especially ytterbium and yttrium silicates are promising candidates due to their matching CTE, outstanding chemical compatibility with SiC, excellent high-temperature stability, and low recession in water vapor environments. The RE disilicates ($RE_2Si_2O_7$) have a CTE very close to the SiC/SiC substrate and are thermochemically compatible with the thermally grown SiO_2 (TGO). However, because of higher evaporation in steam due to higher SiO_2 activity, their resistance to volatilization in water vapor is lower than that of the corresponding monosilicate (RE_2SiO_5). Moreover, compared to the RE disilicates, the CTE mismatch of the monosilicates is higher and their thermochemical stability with respect to the SiO_2 TGO is lower, which may cause stresses and decrease the stability of the EBC system by the formation and growth of cracks.[12,16–21]

At operating temperatures above 1200°C, another form of environmental degradation appears in addition to volatilization in water vapor. Silicates, collectively referred to as calcium-magnesium-aluminosilicate (CMAS), can be ingested in turbines with the intake air and are deposited as a glassy phase on components, causing high recessions of SiC or the EBC through chemical corrosion. The CMAS (dust, volcanic ashes, and sand) typically melts above 1200°C and reacts in contact with the EBC, resulting in dissolution-reprecipitation of new low-melting secondary phases with a typical high CTE mismatch to the EBC and the substrate below.

Furthermore, the CMAS melt can infiltrate pores, cracks, and grain boundaries and may thereby induce greater stiffness in the coatings leading to detrimental stress. The reprecipitation of new secondary phases, as well as the thermomechanical stresses, may result in cracking and even partial delamination of the coating. All these types of damage may reduce the protective ability of the coating system due to material recession or by exposing the substrate to corrosive media due to the open channels and cracks. This can result in total failure of the component.[22–26]

A number of studies have investigated the behavior of RE silicate EBCs in contact with CMAS. Grant et al[27] observed the interaction of an yttrium monosilicate pellet (Y_2SiO_5, YMS) with 33%CaO-9%MgO-12%Al_2O_3-45%SiO_2 (mol%) at 1300°C. They described a significant recession of YMS (~100 μm after 10 hours) and the formation of the secondary phase oxyapatite $Ca_2Y_8(SiO_4)_6O_2$. Jang et al[28] used the same CMAS composition to investigate the reaction of ytterbium monosilicate (Yb_2SiO_5, YbMS) at 1400°C. In their survey, the recession of YbMS was ~90 μm after 48 hours, indicating a lower recession rate of YbMS compared to YMS. In contrast to these results, Jiang et al[29] found that at 1200°C, YMS exhibits superior CMAS resistance compared to YbMS after 4 hours.

Zhao et al[30] investigated the CMAS resistance of YbMS compared to ytterbium disilicate ($Yb_2Si_2O_7$, YbDS) at 1300°C, depending on the duration of the test for between 1 hour and 100 hours. They concluded that YbDS showed slightly better CMAS resistance than YbMS because of a reduction of diffusional transport through an accumulation of Si at the reaction front in the case of YbDS. The results of Stolzeburg et al[31] support this hypothesis. They stated that the activity of Yb_2O_3 in YbMS was higher than in YbDS and that this leads to a higher material recession. In contrast, Poerschke et al[25] suggested that because of a higher consumption of CaO from the melt, accompanied by an earlier CMAS reaction stop, the monosilicate exhibited better CMAS resistance than the disilicate.

In a further investigation, Liu et al[32] examined the recession behavior of different RE disilicates, including YDS and YbDS. Their results showed the superior resistance of YDS to a standard CMAS (33%CaO-9%MgO-12%Al_2O_3-45%SiO_2) at 1400°C for 10 hours. Liu et al[32] reported higher CMAS resistance of YDS than YbDS, whereas Turcer et al[33,34] showed completely different behavior of these two RE disilicates. They pointed out that the resistance of YbDS was higher compared to YDS because of the smaller ionic radius, which displayed a lower tendency to build the secondary phases.

In recent studies, Stokes et al[35] and Summers et al[36,37] noted the high impact of the Ca:Si ratio in the CMAS compositions on the resulting reaction product. Both reported that with increasing Ca:Si ratio, the formation of apatite $Ca_2RE_8(SiO_4)_6O_2$ phases as the primary reaction product is promoted. In addition, the recession became more pronounced as more RE silicate material was necessary to stop the CMAS attack.[35,37] Furthermore, Stokes reported that at high Ca:Si ratios above 0.72 only apatite is formed and that for lower ratios the silicates of smaller RE cations, such as Yb, have a tendency to form additional metastable reaction products.[35]

Comparing these studies, the factors dominating the reaction rates remain unclear and a ranking with respect to stability concerning CMAS-induced recession cannot be

TABLE 1 Examples of experimental parameters from different CMAS studies

Source	Temp. °C	Ca:Si ratio	CMAS quantity mg/cm^2	Duration h	Material
Grant et al[27]	1300	0.73	12-13	1,4,24,100	YMS
Jang et al[28]	1400	0.73	40	2,12,48	YbMS
Zhao et al[30]	1300	0.73	30-35	1,4,24,100	YbDS, YbMS
Jiang et al[29]	1200	0.73	No inform.	4	RE-MS
Liu et al[32]	1400	0.73	314	10	YbDS, YDS
Ahlborg et al[38]	1500	0.73	40 + 40 mg/50 h	5,50,100,150,200	YbMS, YDS
Poerschke et al[39]	1300	0.77	18-19	0.16;4,24	-
Turcer et al[33,34]	1500	0.76	15	96	i.a. YbDS, YDS
Stolzenburg et al[31]	1300	0.73	35	96	YbDS, YbMS
Stokes et al[35]	1200-1400	0.64; 0.48; 0.096	50% CMAS pellet	1,10,50	YbDS, YDS
Summers et al[36,37]	1300	0.72; 0.33; 0.14	18	10,250	YDS, YMS

established. The discrepancies in the observations could be explained by the different experimental parameters used (Table 1). Besides the aspects noted in the table, different sample preparation was used in the studies, which may also explain the different results.

Table 1 indicates that no previous study has examined the CMAS resistance of the ytterbium- and yttrium-based silicates under identical experimental conditions. The major objective of the present study is the comparative examination of the CMAS resistance of the four different RE silicates (YbMS, YbDS, YMS, and YDS) by testing the materials under exactly the same conditions. This includes sample production, preparation, and the CMAS test as well as the characterization of the results.

Furthermore, it will be considered whether it is possible to combine the positive EBC-relevant properties of YbDS and YbMS in a single compound material to create a material with well-matching CTE and simultaneously increased resistance to CMAS and water vapor corrosion. Therefore, in addition to the four pure RE silicates, three mixtures of YbMS and YbDS, in the following designated YbMix, are examined with respect to their CTE and their resistance to CMAS corrosion. The three silicate mixtures exhibit a low (YbMix1), medium (YbMix2), and high (YbMix3) percentage of YbMS in comparison to YbDS.

2 | MATERIALS AND METHODS

2.1 | EBC pellet processing

Commercial powders of YbDS, YbMS, YDS, and YMS from Oerlicon Metco (US) Inc were utilized to produce the experimental samples. The powders were ball milled with zirconia balls in ethanol for 48 hours to ~1 μm, dried, and sieved. To produce the Yb silicate mixture samples, the YbMS and YbDS powders were blended in three different ratios and homogenized in a tumbler for 24 hours. The seven powders were loaded separately into graphite dies (Ø = 20 mm) surrounded by graphite foil, pressed and densified under vacuum via field-assisted sintering (FAST) in an HP-D5 device (FCT Systeme GmbH). The FAST parameters were 30°C/min heating rate up to 1500°C, 5 minutes holding time, −10°C/min cooling rate, and a pressure of 50 MPa. Two samples of each investigated material were produced in this way. After the sintering process, the graphite foil around the densified samples (5 mm thick) was removed and the surface of the samples was ground and polished to Ra = 1 μm surface roughness with standard metallographic techniques. The density and the microstructure of the pellets were determined by analyzing the microstructure of the as-sintered samples via image analysis software AnalySIS pro (Olympus Europa SE & Co. KG). For this analysis, the samples were cut by a slow-speed diamond saw and cold mounted into epoxy resin (EpoFix, Struers). The cross section was polished to 1 μm for further investigation. In order to accurately determine the porosity, 15 images of areas in the center, at the edge, and in the region in between were examined.

Bar samples were produced of all investigated materials to determine the CTE. The milled powders were filled into a metal die (40 × 5 × 5 mm), cold isostatic pressed and sintered in air for 4 hours at 1500°C. After cooling, the surface of the sintered samples was ground to 1 μm surface roughness and dried in a drying chamber at 120°C to evaporate the remaining water.

2.2 | CMAS application and corrosion test

The chemical composition of the CMAS used in this study is 50%SiO_2-38%CaO-5%MgO-4%Al_2O_3-1%Ka_2O-1%Na_2O-1%Fe_2O_3 (mol%). This CMAS composition was selected

because of its similarity to the chemical composition of desert sands with a high Ca:Si ratio (0.76).

The CMAS was synthesized by mixing $CaCO_3$, MgO, Al_2O_3, Na_2CO_3, K_2CO_3, and Fe_2O_3 into a base of amorphous colloidal silica LUDOX AM (Sigma Aldrich). After mixing, the powders were placed in an alumina crucible and heated to 1400°C in a box furnace Naberterm-HT0817 (Naberterm) for 6 hours. The alumina content of the initial weight was reduced by 0.5 wt% to compensate for interdiffusion with the material of the crucible. After quenching the melt in ice water, the resulting glass was dried, ball milled, and sieved to obtain a powder fraction below 25 μm.

This CMAS composition was homogeneously applied as a slurry (based on ethanol) to the polished surfaces of the bulk samples with a surface weight of 20 mg/cm^2. The specimens were placed in a drying chamber for 2 hours at 120°C to ensure the evaporation of residues of ethanol and water. After drying, the seven CMAS-coated samples were placed on an alumina plate, and heat treated in air in a box furnace at 1400°C for 8 hours (5°C/min heating and cooling rate). A temperature of 1400°C was chosen to reduce the CMAS viscosity resulting in a higher diffusion activity during the CMAS reaction.[40] In combination with a high Ca:Si ratio of 0.76, the CMAS attack was more aggressive and the material recession could be observed in a shorter experimental time (8 hours). In addition, 1400°C is just below the melting temperature of silicon (1414°C), which is intended to serve as a bond coat in a future application system.

After the test, the CMAS-interacted samples were cut using a slow-speed diamond saw. The partial samples were cold mounted in epoxy resin and the cross sections were polished to 1 μm surface roughness for further investigations.

2.3 | Characterization methods

The starting powders were characterized using an X-ray diffractometer (XRD, D4 Endeavor, Bruker AXS GmbH) to investigate phase composition and to ensure purity. Also, the near-surface regions of the bulk samples were examined by XRD before and after CMAS interaction. The cross sections of reference samples in as-sintered conditions and the samples reacted with CMAS were observed in a scanning electron microscope (SEM; SEM Ultra 55 Carl Zeiss NTS GmbH) equipped with an energy-dispersive spectroscope (EDS). The micrographs were produced at an acceleration voltage of 8 kV and the EDS analyses were produced at 15 kV acceleration voltage. The penetration depth and RE enrichment during the CMAS interaction test were characterized by EDS elemental mapping for Ca and the RE elements Y and Yb using the INCA software from Oxford Instruments (Oxford Instruments NanoAnalysis & Asylum Research).

For CTE determination, the 25 mm bar samples were examined in a dilatometer 402 C (Erich Netzsch GmbH & Co. Holding KG) calibrated with high-purity single-crystal Al_2O_3. The tests were performed between 25°C and 1200°C using heating and cooling rates of 3°C/min with a holding time of 30 minutes.

3 | RESULTS

3.1 | Thermal expansion

The CTE of the seven test materials examined by dilatometry is presented in Table 2. In accordance with the literature, the disilicates exhibit a lower CTE (4.8×10^{-6}/K for YbDS and 4.5×10^{-6}/K for YDS) than their monosilicate equivalents (7.2×10^{-6}/K for YbMS and 6.9×10^{-6}/K for YMS).[41-43] These results confirm that the CTE of these disilicates is closer to the SiC/SiC substrate (4.7×10^{-6}/K) than the CTE of the monosilicate.[44] In comparison to the literature, the order of CTE values is confirmed, but they are slightly higher.

With respect to the CTE of the three silicate mixtures, it is evident that the CTE rises with an increased fraction of monosilicate. The CTE of YbMix1 (5.7×10^{-6}/K) with a small amount of monosilicate is close to the CTE of the pure YbDS sample. The CTE of YbMix3 (6.7×10^{-6}/K) is closer to that CTE of the pure monosilicate sample, while the CTE of YbMix2 (6.1×10^{-6}/K) is midway between the CTE of YbMS and YbDS.

3.2 | CMAS resistance test

The SEM image and the XRD pattern of the untreated YbMS and YbDS bulk samples are shown as examples of the pure silicate samples in Figure 1. The image analysis indicates a porosity of $1 \pm 0.4\%$ for the YbMS sample and a porosity of $2 \pm 0.8\%$ for the YbDS sample.

TABLE 2 Experimentally measured CTE and literature references for ytterbium, yttrium silicates, and SiC

Source	$Yb_2Si_2O_7$ $\times 10^{-6}$/K	Yb_2SiO_5 $\times 10^{-6}$/K	$Y_2Si_2O_7$ $\times 10^{-6}$/K	Y_2SiO_5 $\times 10^{-6}$/K	YbMix1 $\times 10^{-6}$/K	YbMix2 $\times 10^{-6}$/K	YbMix3 $\times 10^{-6}$/K	SiC $\times 10^{-6}$/K	CMAS $\times 10^{-6}$/K
Experimental	4.8 ± 0.2	7.9 ± 0,4	4.5 ± 0,3	7.5 ± 0.4	5.7 ± 0.3	6.1 ± 0.29	6.7 ± 0.3	—	—
Literature	3.7-4.5[41]	7.2[42]	3.9[19]	6.9[42]	—	—	—	4-5.5[44]	~10[45,46]

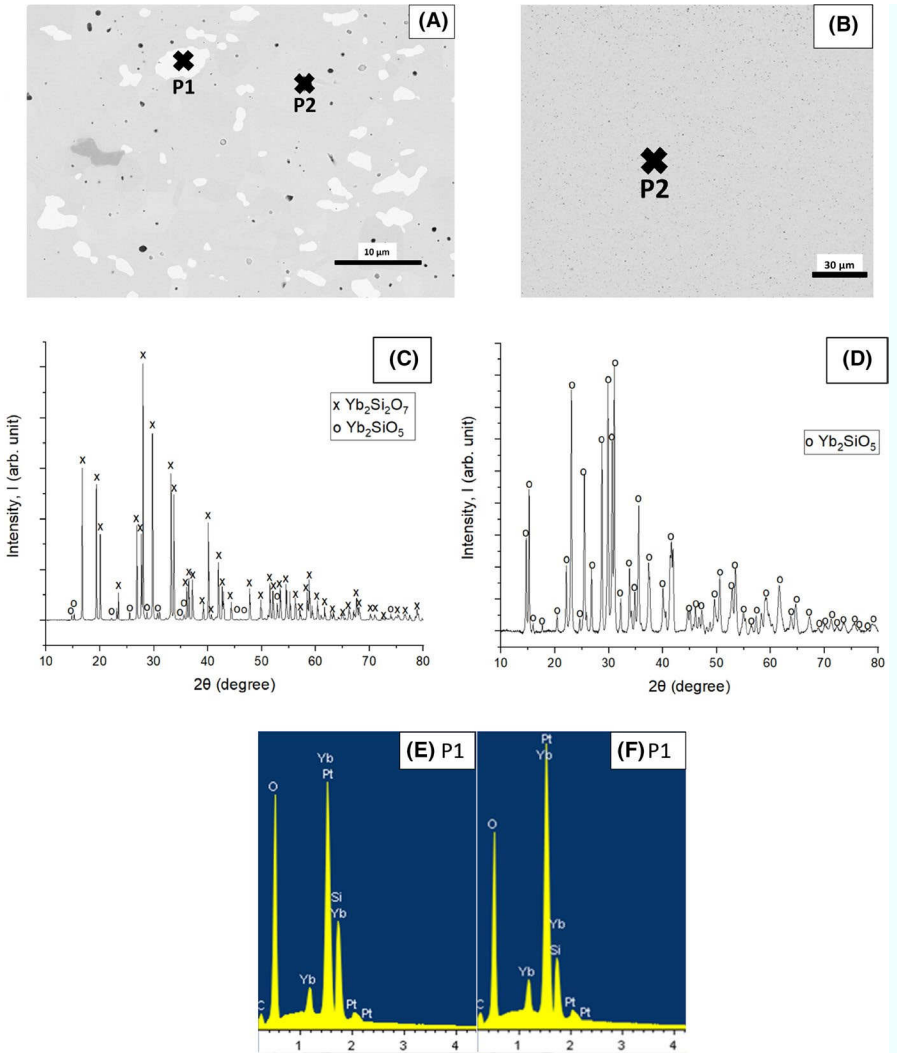

FIGURE 1 SEM images and XRD patterns of the ytterbium disilicate (A, C, E) and monosilicate (B, D, F) bulk samples before the CMAS interaction test. Results of EDS analysis at representative positions P1 and P2 are given in subfigures E and F [Color figure can be viewed at wileyonlinelibrary.com]

Associated XRD patterns, except for YbDS, can be fully indexed by the respective crystalline phase and no amorphous background is observed. For the YbDS sample, the pattern indicates YbMS as a secondary phase (Figure 1C). The Rietveld analysis reveals a monosilicate amount of ~5%. The coexistence of these phases is also visible from Figure 1A. The EDS identifies the phase of brighter contrast as enriched in silicon while the darker phase contains less silicon (Figure 1E,F). In addition to the rare earth silicates, a platinum peak is evident in Figures 1, 2, 8, and 9. This is related to a sputtered platinum layer which was applied to the sections to enhance conductivity for the SEM.

The SEM and XRD patterns for the YbMix bulk samples with low and high amounts of YbMS are shown as examples of the YbMix samples in Figure 2. An image analysis of 15 pictures per sample indicates a sample porosity of $2 \pm 0.7\%$. As expected, the XRD patterns can be attributed to YbDS and YbMS for all compositions (Figure 2C,D). Observing the microstructure in Figure 2A,B, the structure appears to be rather homogeneous. However, some larger disilicate or monosilicate islands were identified (Figure 2A,C,E,F).

Figure 3A,B shows a cross section of the YbDS sample after CMAS interaction at 1400°C for 8 hours. Three phases are visible due to the different brightness in the SEM image (Figure 3B) after the interaction of CMAS. An acicular phase is formed between the remaining CMAS and the YbDS pellet. The reaction layer consists of different features. Needle and bulky objects are visible. The remaining CMAS phase is observable between the individual needles. The thickness of the reaction layer is ~100 µm. In addition to the formation of the different phases, vertical cracks also appear. These cracks extend from the surface of the CMAS reservoir on top of the specimen through the reaction layer to the interface between the pellet and reaction layer. Figure 3C,D illustrates the microstructure of the YbMS sample after the CMAS interaction test. Compared to the YbDS, the observed reaction layer in the YbMS is thinner and exhibits finer and shorter needles. Furthermore, a dense fringe is visible at the interface between the pellet and reaction layer. This fringe and also the needles consist of apatite. The remaining CMAS is

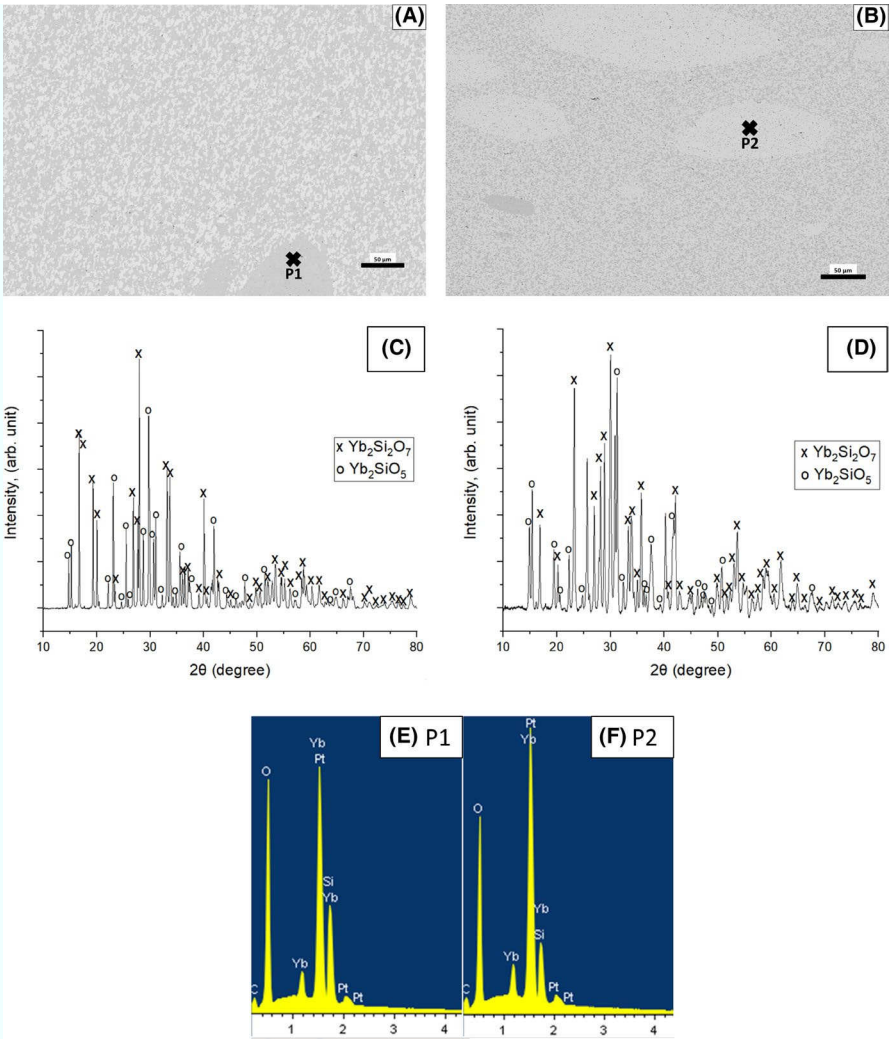

FIGURE 2 SEM images, XRD pattern of the YbDS-YbMS mixture samples with low (A, C) and high amounts of YbMS (B, D) before the CMAS interaction test and the EDS analysis of YbDS (P1; E) and YbMS (P2; F) islands [Color figure can be viewed at wileyonlinelibrary.com]

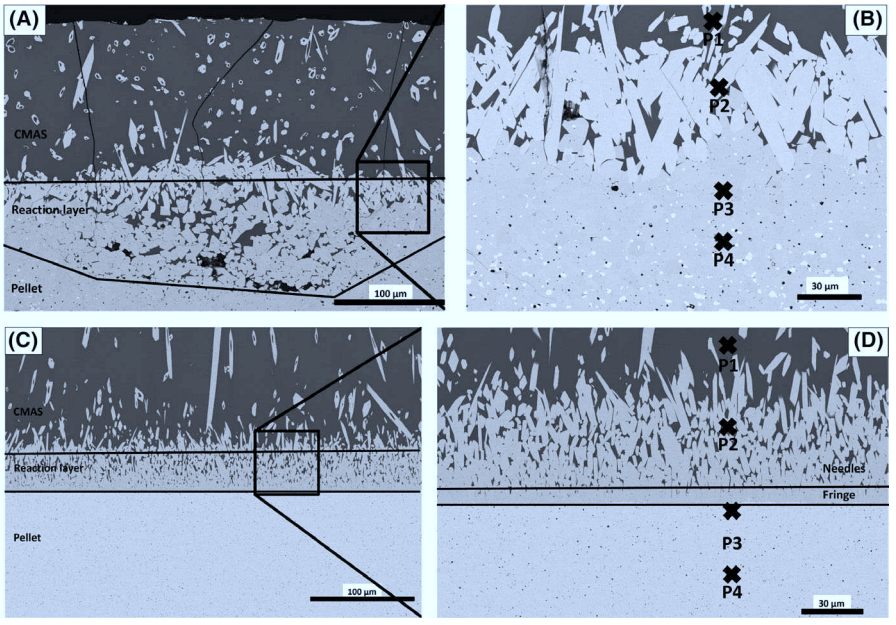

FIGURE 3 SEM images of the pure Yb silicate samples after CMAS interaction at 1400°C for 8 h: YbDS (A, B), YbMS (C, D). EDS analysis was performed at the indicated positions (see below)

visible between the needles. In contrast to the YbDS sample, no cracks can be observed. The average thickness of the reaction layer in the YbMS sample is ~45 µm.

SEM images of the YDS sample after the CMAS interaction test are presented in Figure 4A,B. The difference to the YbDS specimen is clearly visible. The reaction layer is

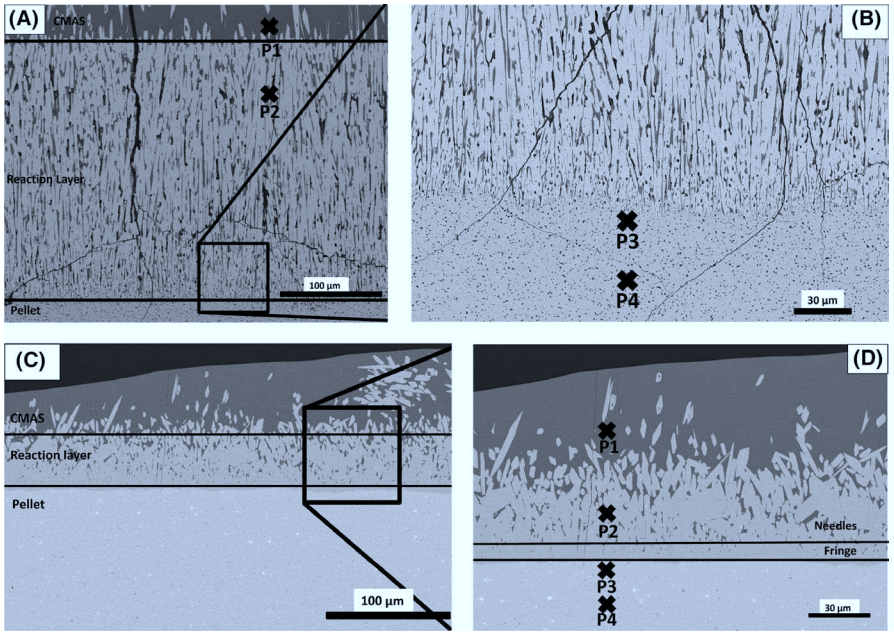

FIGURE 4 SEM images of the pure Y silicate samples after CMAS interaction at 1400°C for 8 h: YDS (A, B), YMS (C, D). EDS analysis was performed at the indicated positions (see below)

FIGURE 5 SEM images of the different material samples after CMAS interaction at 1400°C for 8 h: YbMix1 (A, B), YbMix2 (C, D), YbMix3 (E, F). EDS analysis was performed at the indicated positions (see below)

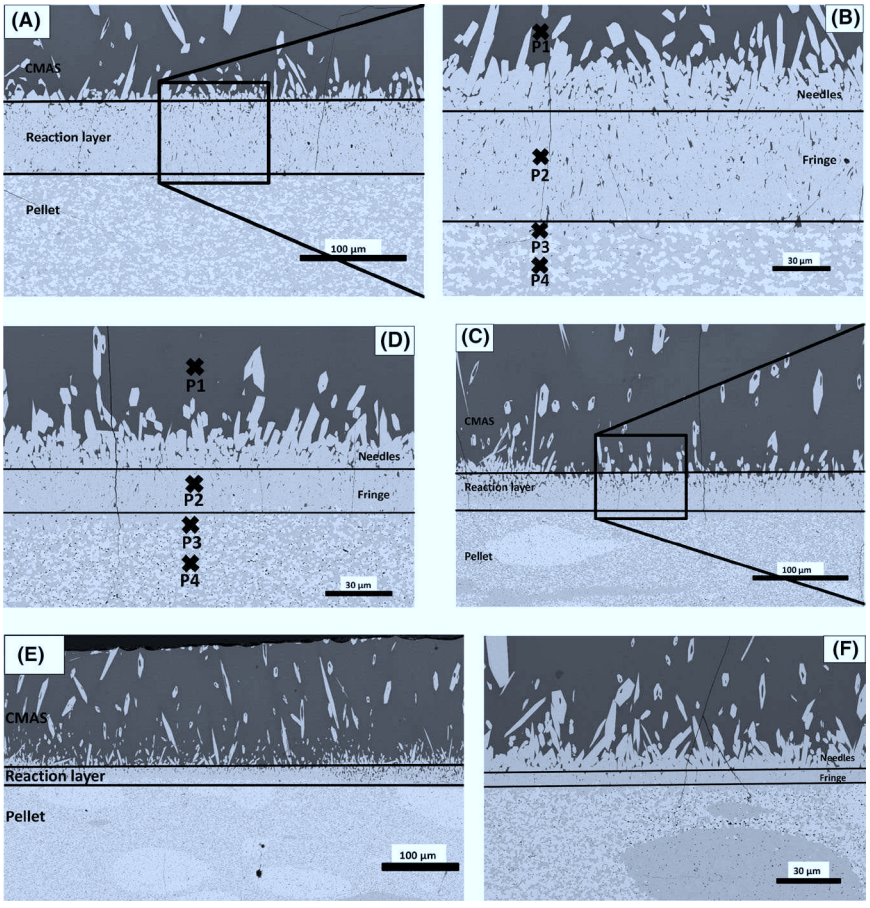

thicker, and the needles have a higher aspect ratio. Also long cracks are evident in the reaction layer. The cracks continue through the whole reaction layer and extend into the pellet below. The reaction layer contains cracks, but the cracks end in the silicate material and are partially connected to each other, which results in a network of cracks (Figure 4B). As in the reaction layer of the ytterbium silicate samples, the remaining CMAS is also visible between the needles in the reaction layer. The average thickness of the reaction layer is ~250 µm.

Figure 4C,D shows the microstructure of the YMS sample after the CMAS interaction test. In contrast to the YDS sample, the reaction layer with YMS includes shorter needles, which are partially connected and resemble the microstructure observed in the YbMS sample. As in the microstructure of the YbMS reaction layer, a thin fringe is visible. The remaining CMAS in between the needle-shaped precipitates in the reaction layer is obvious from the dark contrast. The average thickness of the reaction layer is ~88 μm.

The microstructure of the first ytterbium silicate mixture material YbMix1 (low amount of YbMS) is shown in Figure 5A,B where apparent differences are revealed. The reaction layer is denser than the reaction layers of the pure silicates. The needle structure is only visible at the top of the reaction layer. All interspace gaps between the needles are filled with CMAS. The average thickness is ~82 μm. In contrast to the pure ytterbium silicate samples, the vertical cracks in the YbMix samples extend through the reaction layer into the unreacted sample. Furthermore, in the interface region, the YbMix pellet is homogeneous and no agglomeration can be observed.

Figure 5C,D shows the microstructure of the YbMix2 sample with a medium amount of YbMS. In contrast to the YbMix1 sample, it can be observed that areas of agglomeration also extend up to the pellet interface. Incomplete breakup may be a reason for these agglomerations. Three different reaction layers appear. At locations where areas of YbMS agglomeration extend up to the interface, the needles are longer and a small fringe can be observed (Figure 5E right). In the case of an YbDS agglomeration, the reaction layer, as in the YbMix3 sample described later (Figure 6), is much larger with long needles but without a dense fringe. At locations where the Yb silicate mixture is homogeneously blended, the needles are shorter, but the fringe is thicker. The remaining CMAS is found in the gaps between the needles in the upper part of the reaction layer while this is not observed in the fringe directly at the interface where only pores can be observed. The average thickness of the reaction layer is ~38 μm, which is thinner than the reaction layer on top of the pure monosilicate sample.

The microstructure of the reaction layer of the YbMix3 sample with a high amount of YbMS is shown in Figure 5E,F. The reaction layer also displays an inhomogeneous structure. In homogeneously mixed areas, the reaction layer is thin and presents a compact needle structure with a dense fringe. In areas with agglomerated YbMS, the reaction layer is thicker and presents longer needles in comparison to the reaction layer above the homogeneously mixed material. In addition, the structure of the layer is less dense. The reaction layer above the areas with agglomerated YbDS shows a different structure (Figure 6A). It can be observed that the reaction layer is thicker compared to the reaction layer in areas with the appropriate mixture. The structure formed above the YbDS areas exhibits large needles and a large gap which is filled with CMAS. Again, CMAS is only found between the needles but not in the fringe. The reaction layer above the YbMS agglomeration (Figure 6B) displays a thin, dense fringe and a higher proportion of the needles cluster above with CMAS between the needles. The average thickness of the reaction layer above the YbMix3 sample is the lowest measured value in this study at 21 μm.

The XRD pattern for the yttrium and ytterbium silicate samples after the CMAS interaction presented in Figure 7 indicates different phases, which can be assigned to the CMAS residues ($CaSiO_3$, $CaSiO_4$, and $CaFeO_3$) and the reaction phase. In the case of the yttrium silicates, the reaction phase can be attributed to yttrium apatite $Ca_2Y_8(SiO_4)_6O_2$. In the case of the ytterbium silicate samples, the pattern cannot be identified because of a lack of PDF cards in the XRD catalog. However, because of the EDS measurement and the ternary phase diagram of earth alkali metals, rare earth oxides, and silicon oxides, different possible reaction products such as apatite ($Ca_4RE_6(SiO_4)_6O_2$), CaRE cyclosilicate ($Ca_3RE_2Si_6O_{18}$), silicocarnotite ($Ca_3RE_2Si_3O_{12}$), and anorthite ($CaAl_2Si_2O_8$)[25,47] are likely to be considered. By comparing the peak positions in the XRD of the present study with the results from Ahlborg et al,[38] the second phase in the present study could most probably be attributed to apatite ($Ca_4RE_6(SiO_4)_6O_2$), which exhibits similar peak positions. This attribution is also supported by the work of Stokes et al,[35] in which they report the absence of extraneous phases other than Yb apatite in contact with CaO-rich CMAS and a temperature above 1400°C. In addition, the experimental and modeling studies of Summers et al[36] also indicate that in contact with CaO-rich CMAS only apatite is formed in contact with RE silicates.

The chemical composition was analyzed by EDS at the four points marked in Figures 3-5. The results of this analysis

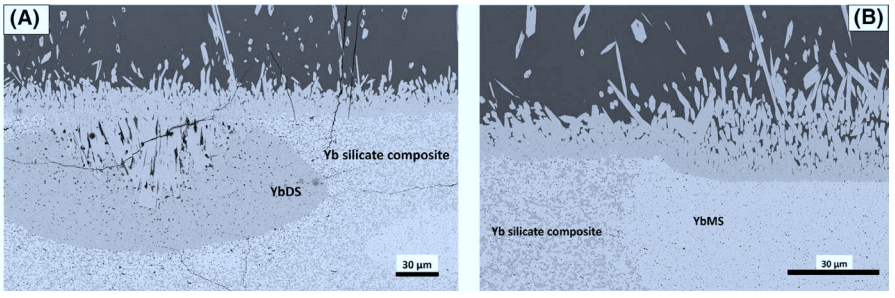

FIGURE 6 Areas of YbDS (A) and YbMS (B) agglomeration in the Yb silicate mixture with high amounts of YbMS after CMAS interaction at 1400°C for 8 h

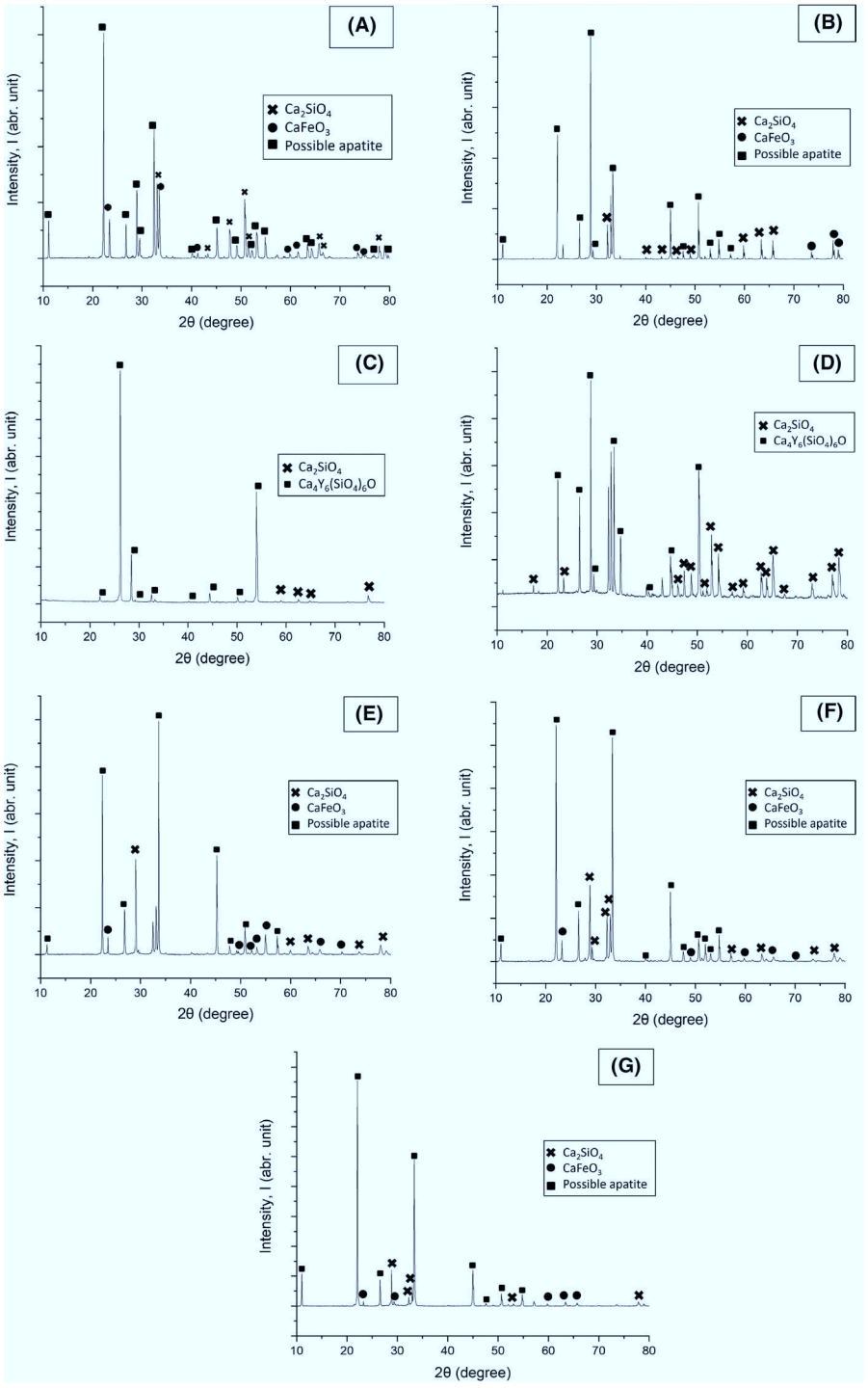

FIGURE 7 XRD pattern of the different material samples after CMAS interaction at 1400°C for 8 h: YbDS (A), YbMS (B), YDS (C), YMS (D); YbMix1 (E), YbMix2 (F), and YbMix3 (G)

are illustrated for the ytterbium silicate materials in Figure 8. In the remaining CMAS reservoir on top of the reaction layer (P1), the CMAS elements Ca, Al, Mg, Fe, Si, O, K and a low amount of Yb are verified. In the reaction layer (P2), the amount of Yb is greater, and furthermore, only Ca, Si, and O are detectable. At the interface between the reaction layer and the remaining Yb silicate pellets (P3), only Yb, Si, and O are verified and no Ca is detectable. The same composition is measured inside the Yb silicate pellets (P4). Results for the yttrium silicate samples are shown in Figure 9. The results are similar to those of the ytterbium silicates, except for the dedicated RE element (Y instead of Yb).

4 | DISCUSSION

4.1 | Pure RE silicates

The results of this comparative study of the pure yttrium and ytterbium silicates show distinct differences between

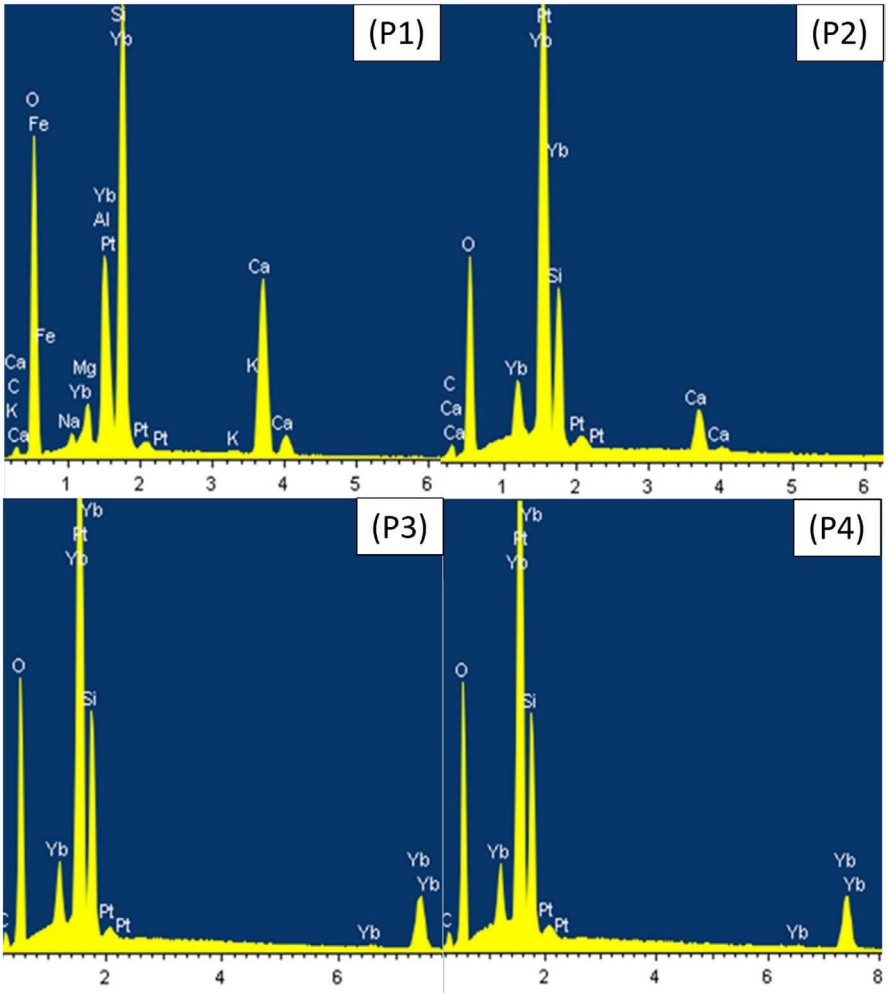

FIGURE 8 Typical EDS patterns of the ytterbium silicate samples at exemplary positions labeled in Figure 3 (YbDS, YbMS) and Figure 5 (YbMix1, YbMix2 and YbMix3) after the CMAS interaction test at 1400°C for 8 h; remaining CMAS (P1), the reaction layer (P2), below the interface (P3) and in the remaining pellet (P4) [Color figure can be viewed at wileyonlinelibrary.com]

mono- and disilicates as well as between silicates with different RE cations (Yb^{3+} and Y^{3+}). From the thickness of the reaction layer with CMAS, presented in Table 3, it is clearly visible that both investigated ytterbium silicates, YbDS and YbMS, exhibit a lower layer thickness than their yttrium silicate counterparts (YDS and YMS). This indicates a lower recession of ytterbium silicates under CMAS attack compared to the yttrium silicates.

A possible explanation put forward by Krause et al[48] and Turcer et al[34] is based on the differences in optical basicity caused by the different ionic sizes of Yb^{3+} (0.985 Å) and Y^{3+} (1.019 Å). Optical basicity (OB), first used by Duffy et al,[49] describes the chemical activity of oxides in glass and is related to the ability of an O^{2-} anion to donate electrons to given cations. Hence, this property depends on the extent to which the respective cation can be polarized. Using the Lewis acid-base theory, which defines bases as electron donators and acids as electron acceptors, the reactivity between a crystalline oxide and an oxide glass tends to increase with an increased difference in their OB. The evaluation of the different OBs from the studies of Duffy et al[50,51] indicates that the basicity of Yb_2O_3 (0.94) is lower than its yttrium counterpart (1.0). This could be an indication that ytterbium silicates exhibit a lower reactivity in contact with CMAS with a basicity of 0.64, which may lead to a lower recession. It should be taken into account that the OB difference is only a first indication which influences the reactivity and does not include other factors, for example, the local concentration of species.[34,48,52]

Another explanation for the different behavior is presented by Felsche et al.[53] Normally, a Ca:Re ratio of 1:4 is needed to form apatite. But in their work, they showed that apatite is metastable in REO1.5-SiO2 systems with smaller RE^{3+} cations. The authors concluded that a higher amount of larger cations such as Ca^{2+} are needed to stabilize the apatite in the case of ytterbium.[53] In this case, more CaO is consumed for the reaction with Yb silicates than with Y silicates. As the Ca:Si ratio decreased, Stokes et al[35] postulated that the amount of apatite formed with the different RE silicates decreases, which they attributed to the reduced apatite stability for smaller RE cations such as ytterbium and yttrium. Furthermore, in their work, Stokes et al reported that YDS forms overall more apatite than YbDS.[35] Therefore, the lower reactivity with CMAS, indicated by the smaller OB mismatch, the higher amount of CaO needed to form stabile apatite and the precipitation of certain phases at lower Ca:Si

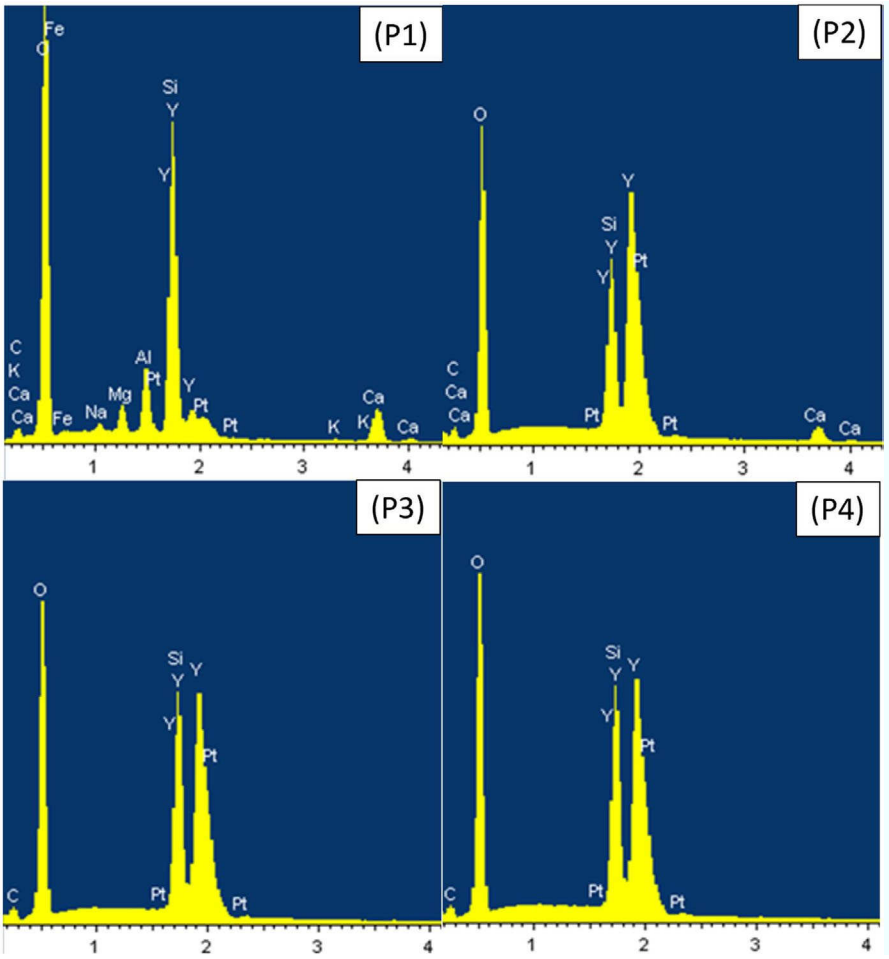

FIGURE 9 Exemplary EDS pattern of the yttrium silicate samples (YDS and YMS) at the four analyzed positions in Figure 4 after the CMAS interaction test at 1400°C for 8 h; in remaining CMAS (P1), the reaction layer (P2), below the interface (P3), and in the remaining pellet (P4) [Color figure can be viewed at wileyonlinelibrary.com]

YbDS µm	YbMS µm	YDS µm	YMS µm	YbMix1 µm	YbMix2 µm	YbMix3 µm
100 ± 6	43 ± 4	255 ± 9	88 ± 14	82 ± 9	38 ± 11	21 ± 18

TABLE 3 Reaction layer thickness of the seven material candidates after the CMAS interaction test at 1400°C

ratios may explain the thinner apatite layer in the case of the Yb silicate samples.

The results of the CMAS interaction tests show a consistently lower recession of the monosilicates with respect to CMAS, compared to the disilicates (Table 3). Poerschke et al,[25] who also observed the tendency that monosilicates display better CMAS resistance, explain this behavior using the following reaction equations, in which RE represents, unlike the previous case, the rare earth oxide, S the silica, and C the calcium oxide:

$$RE_{0.5}S_{0.5} + 0.125C_{deposit} \rightarrow CaO_{0.125}REO_{0.5}S_{0.375} + 0.125S_{deposit}, \quad (1)$$

$$RE_{0.67}S_{0.33} + 0.167C_{deposit} + 0.167S_{deposit} \rightarrow 1.33C_{0.125}RE_{0.5}S_{0.375}. \quad (2)$$

Poerschke et al[25] postulated that according to Equation 1, disilicates consume CaO from the melt to build apatite while at the same time releasing SiO_2. This reaction changes the volume of the melt slightly. The process will continue until the melt is depleted in CaO, which is a major driving force of the reaction. In contrast, the process of dissolution of the monosilicate followed by the precipitation of apatite, shown in Equation 4, consumes CaO as well as SiO_2 from the CMAS melt. This results in a quicker local depletion of Ca^{2+} and a volume reduction of the remaining melt.[25]

From another perspective, Equations 3 and 4 postulate that for the bonding of the same amount of $CaSiO_3$, which can be considered as a component in CMAS, in the apatite phase, around 50% more disilicate than monosilicate is necessary. Grant et al[27] describe why within the same time the disilicate reacts to a thicker and more volumetric reaction layer than the corresponding monosilicate.

One effect of the differences in the volume change can be observed from Figure 3B,D. The volume of the melt between the apatite grains is larger in the case of the DS than for the MS. This might facilitate continued inward diffusion and thus material recession. Poerschke et al[25] report that the resulting surface recession of the disilicates is twice as high

compared to their monosilicate counterparts. Theoretically, the apatite reaction results in an enrichment of Al_2O_3, MgO, Fe_2O_3, K_2O, and Na_2O, which could trigger an intrinsic crystallization of the remaining melt to different crystalline phases.[25] Only the EDS measurement of the remaining melt, presented in Figures 8A and 9A, revealed the different components (Fe, Al, K, Na, Mg). This may indicate an increased concentration of these components in the remaining CMAS melt.

A further reason for the slower recession of monosilicates could be the change in viscosity during the reaction. Previous publications showed that the viscosity of the melt is increased by increasing the RE concentration or the Si content.[36,54,55] According to the work of Opila et al,[56] it could be concluded that with increasing viscosity, the diffusion activities decrease and therefore the reaction slows down. Also, in highly viscous CMAS melt, the flow rate of the melt into the coating material would be reduced.[23] In addition, Krämer et al[57] showed that the depth of penetration decreases with higher viscosity. Since dissolution of monosilicate leads to an increase of the RE content and a higher consumption of CaO compared to the disilicates, it could be concluded that the viscosity increases more rapidly. As a consequence, in the monosilicate CMAS reaction, the diffusion activity, the flow rate of the melt into the coating as well as the depth of CMAS penetration would decrease more sharply over time than in the disilicate CMAS reaction, resulting in minor recession.

Another factor influencing the recession behaviors of mono- and disilicates in contact with CMAS might be the presence and morphology of a fringe at the interface between the monosilicate and the corresponding reaction layer. The fringe can be observed for YbMS and YMS (Figure 3C,D; Figure 4C,D), but is not present in case of YbDS and YDS (Figure 3A,B; Figure 4A,B). Zhao et al[30] also reported the incidence of this fringe in the case of YbMS. They attributed the formation of the fringe to an accelerated saturation of the melt by Yb_2O_3, which is driven by the higher activity

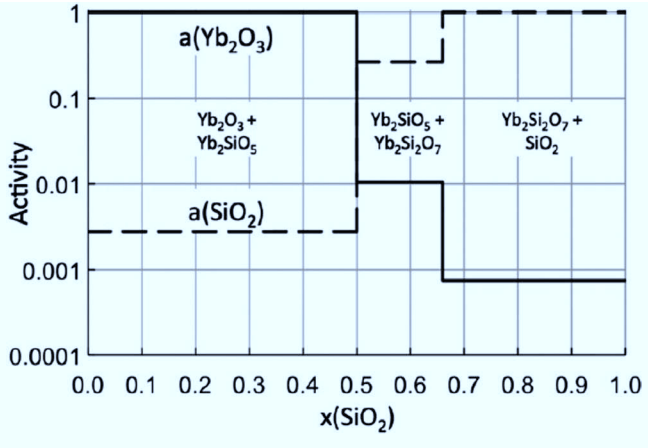

FIGURE 10 Measured activity of SiO_2 and calculated activity of Yb_2O_3 based on References [31, 58]

of Yb_2O_3 in YbMS compared to YbDS (Figure 10,[58]). In contrast, the absence of a fringe in the case of YbDS was attributed to the higher volume of intergranular melt in the reaction layer, which may prevent the formation of a dense apatite fringe.[30] With respect to recession, it can be assumed that the dense fringe acts as a protective layer against CMAS infiltration or Ca^{2+} diffusion. This assumption is supported by the results of Summers et al.[37] They observed a dense fringe at the interface of the reaction zone and remaining YbMS as well as reduced recession of the MS, which was only 50% of the amount they predicted.

Vertical cracks can be observed in the SEM micrographs of pure RE silicate samples. In comparison, the density of cracks is higher in the disilicates than in the monosilicates. Two different reasons may lead to these cracks. As mentioned above, the differences in CTE of the remaining CMAS (9.8×10^{-6}/K),[46] of the apatite reaction layer (7.5×10^{-6}/K),[59] and of the disilicate pellet ($4.5\text{-}4.8 \times 10^{-6}$/K) result in stresses on cooling down. Because of the minor CTE mismatch between the monosilicates and the CMAS, the resulting stresses are smaller, thus inducing fewer cracks.

A second explanation is the penetration of CMAS into grain boundaries. Turcer et al[33] suggested in their study that the driving force for this penetration is the reduction of the total energy of the system, due to a preferred formation of ceramic/glass interfaces instead of ceramic/ceramic interfaces. This might be possible because in a high-angle grain boundary, the grain boundary energy γGB is twice as high as the ceramic/glass interface energy γI.[60,61] Turcer et al[33] postulated that the penetration of the grain boundaries by the CMAS melt results in the dilatation of the material, termed the blistering effect. When the CMAS-infiltrated region expands above the unaffected areas a dilation gradient appears, which results in compression stresses. The compression increases with the thickness of the infiltrated top region. When the stress level exceeds a critical value, crack deflection may occur.

In contrast to the findings of Turcer et al,[33] the EDS measurement does not detect CMAS elements in the areas close to the cracks inside the pellets. By comparing the crack frequency, it can be seen that the disilicate samples exhibit the highest number of cracks. In the Yb silicate mixture materials, the crack frequency decreases with increasing amount of YbMS, which indicates that an increased proportion of YbMS suppresses the vertical cracking. This decreasing trend continues with the pure monosilicate samples. For this reason, it may be assumed that in the present study, stresses induced by the CTE mismatches between the apatite phase and the remaining substrate contribute to crack formation. The increased CTE of the pure monosilicates and the YbMix samples with an increased amount of monosilicate may reduce these stresses and therefore the crack frequency.

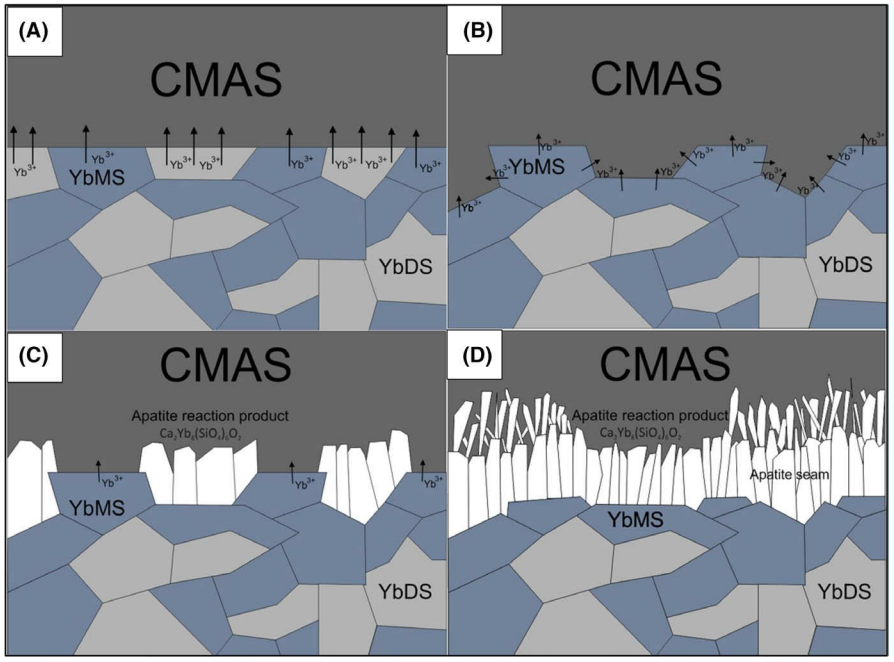

FIGURE 11 Schematics of the reaction mechanisms between CMAS and Yb silicate mixtures [Color figure can be viewed at wileyonlinelibrary.com]

4.2 | Disilicate and monosilicate mixed materials

The CTE of the Yb silicate mixtures was determined to evaluate their suitability as EBC materials for SiC CMCs. An increase in the CTE of the Yb silicate mixtures with a higher amount of YbMS is observed (Table 2). Typically, material combinations with a low CTE mismatch are preferred to avoid stress-induced cracking. Therefore, Yb silicate mixtures with a low or medium amount of YbMS (YbMix1 and YbMix2) can be expected to be advantageous in combination with an SiC or SiC/SiC substrate (4-5.5 $\times$ 10^{-6}/K) compared to those with a high amount of YbMS (YbMix3) and especially compared to pure YbMS.

However, in contact with CMAS, it can be observed that the microstructure of the three Yb silicate mixtures exhibits a lower amount of cracks with an increased amount of YbMS. The lower amount of cracks indicates that a higher YbMS fraction in the Yb silicate mixtures causes a lower stress level, due to a smaller CTE mismatch between the Yb silicate mixtures, the remaining CMAS and the apatite layer formed. This hypothesis is also supported by the absence of vertical cracks in the microstructures of the pure monosilicates (Figure 3C,D and Figure 4C,D). Thus, a conflict can be identified. A low CTE is desirable for the EBC to prevent stress-induced cracks at the SiC/SiC substrate/EBC interface. At the same time, a high CTE may prevent cracks in contact with CMAS and apatite and thus increase CMAS resistance. In an EBC system on a flat SiC CMC substrate, the stress conditions are affected by the CTE mismatch between substrate and coating. The CTE of the substrate has a greater influence than the CTE of the thin coating. However, at edges or complexly shaped components, the influence of the EBC CTE increases and should be noted. Therefore, Yb silicate mixtures with a medium proportion of YbMS and an optimized CTE could be promising.

Considering the microstructures (Figure 5) and the thickness of the reaction layer (Table 3), it can be said in summary that with an increased amount of YbMS in the Yb silicate mixture materials, the thickness of the reaction layer in the respective Yb silicate mixture decreases.

It should be emphasized that in the case of the silicate mixtures with medium and high amounts of YbMS, the thickness of the reaction layer is even lower than in the case of pure YbMS. Generally, the better resistance of the Yb silicate mixtures under CMAS attack is also apparent in the different behavior of the regions of YbDS and YbMS agglomeration and of the homogeneously mixed regions (Figure 6A). While the silicate mixtures display a reaction layer with a high proportion of dense fringe, the regions of pure silicate show a more porous and thicker layer. As can be seen in Figure 6B, the reaction layer above the YbMS agglomeration exhibits a thin and dense fringe. However, in comparison to the reaction layers above the homogeneously mixed regions, the proportion of the dense fringe in the reaction layer is smaller. Additionally, the thickness of this reaction layer above the YbMS agglomeration is approximately twice that of the reaction layer above the homogeneously mixed regions. It can be estimated that more of the pure YbMS material was converted into apatite than of the homogeneous silicate mixture material. Compared to the regions of agglomerated YbMS and the homogeneously blended silicate mixture, the reaction layer above the agglomerated YbDS regions is more pronounced and much thicker. The reaction layer appears less dense and the YbDS material below is dissolved to a larger extent.

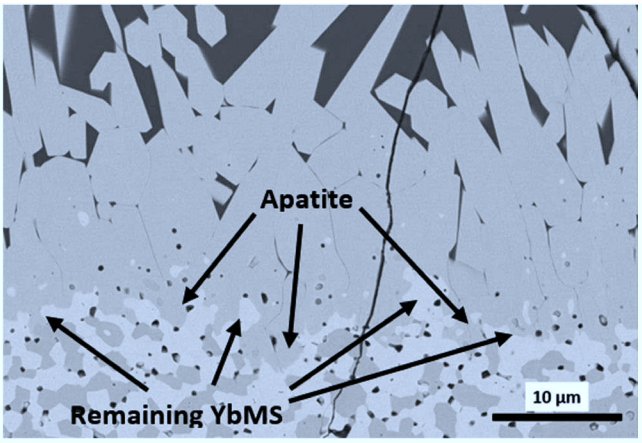

FIGURE 12 SEM close-up of remaining YbMS at the apatite/EBC pellet interface

Several mechanisms may contribute to the superior resistance of the Yb silicate mixtures to CMAS corrosion. The first factor is the differences in the interface layer structure above the mixed and unmixed areas. As mentioned above, the disilicate does not exhibit a dense fringe at the interface. The visible fringe at the interface of the silicate mixtures is thicker compared to the fringe of the monosilicate. However, the proportion of the fringe in the reaction layer seems higher and the structure appears denser compared to the monosilicate layer. This indicates improved protective behavior preventing the CMAS melt coming into contact with the remaining pellet, which may delay the dissolution/precipitation process.

A second hypothesis is illustrated in Figure 11. With respect to the recession stability of the pure silicates and the higher silica activity in YbDS (Figure 10), it can be assumed that the CMAS recession process of the Yb silicate mixtures starts with the preferred dissolution of YbDS into the melt (Figure 11A). Lower stability and thus a potentially higher dissolution rate into the CMAS melt are also indicated by the lower melting temperature of YbDS compared to YbMS. After most of the YbDS has been dissolved at the reaction front, YbMS is now exposed to the CMAS melt with a higher surface area compared to the pure YbMS. This may result in an accelerated dissolution of YbMS in the melt if compared to the reaction in the pure YbMS sample (Figure 11B). In this case, especially in the valleys of the interface structure, the melt will be saturated with Yb^{3+} earlier, which can lead to a higher number of apatite nuclei and earlier apatite precipitation (Figure 11C). Where YbDS and YbMS are homogeneously mixed, a continuous layer can be readily formed from these initial precipitates. This built-up apatite layer is denser than in the case of the pure YbMS reaction layer and may delay the further reaction with CMAS more efficiently (Figure 11D) Because of the distinct build-up times, the reactions become delayed to different extents, resulting in a different reaction layer thickness. It is presumed that a combination of the outlined effects may have led to the observed behavior of the Yb silicate mixtures. Even though the initial assumption appears to contradict Zhao et al,[30] who postulated a higher recession rate of YbMS, our hypothesis is supported by the observation of the remaining YbMS at the pellet/apatite interface (Figure 12), while no YbDS can be detected. In view of the higher temperature in the present study, this may be understood in such a way that dissolution into the CMAS melt is accelerated to a greater degree by the higher silica activity than the formation of apatite is promoted by the increase of Yb^{3+} activity in the local melt.

5 | CONCLUSIONS

Four pure RE silicates and three Yb silicate mixtures were tested for their resistance to CMAS attack and their CTE. It was proven that the RE monosilicates exhibit better resistance to CMAS attack than their disilicate counterparts. This was primarily attributed to the theory that disilicates show a higher recession because their chemical reactions with CMAS stop later compared to their monosilicate counterparts because of a lack of melt volume reduction during the reaction. In addition, the present study suggests that an apatite fringe, which is only formed at the monosilicate/apatite interface, acts as a Ca^{2+} barrier.

Furthermore, this study shows a distinct difference between silicates with different RE cations. The ytterbium silicates generally exhibit a lower recession than the yttrium silicates. This correlates well with the theory that a greater difference in optical basicity between two materials may lead to a higher driving force to dissolve into the CMAS melt and in a second stage to precipitate apatite.

The evaluation of the results of the CMAS interaction test and the CTE measurement for the Yb silicate mixture materials showed that with the addition of YbMS, the CTE of the mixtures increases as expected. Additionally, the resistance to the CMAS increases considerably and is already higher with a medium amount of monosilicate than for the pure YbMS. It is assumed that due to faster and denser apatite precipitation, a protective fringe is precipitated at the apatite/pellet interface which delays a further CMAS attack even more efficiently than the pure ytterbium monosilicate. This suggests that an Yb silicate mixture material with a low to medium amount of YbMS is a promising candidate for an EBC coating.

Although the pellet microstructure and morphology used in this study do not exactly replicate that of a thermal-sprayed EBC, the information regarding material recession under identical conditions derived from these pellet-based tests provides insights into the expected reactions and performances

of coatings. Since the normal EBC thickness is between 100 and 300 μm and the reaction of CMAS with the EBC material is not complete after 8 hours, it can be estimated that the disilicates and monosilicates may not guarantee sufficient protection against CMAS attack over a longer operating time for EBC coatings of typical thickness. In addition to the influences examined in this work, there are also others to be considered. For instance, the viscosity of the melt, the Ca:Si ratio, reaction time, and temperature have an influence on the recession of the EBC materials. For these reasons, it is necessary to extend the research on CMAS reactions on EBCs to include the influence of more parameters and the improvement of the material resistance.

ACKNOWLEDGMENTS

The authors thank C. Vorkötter, A. Dash, M. Kindelmann, D. Koch, W. Scheld, and R. Steinert (all IEK-1, Forschungszentrum Jülich) for their support with the development of the sample production process and the CMAS interaction test. The authors especially thank D. Sebold (IEK-1, Forschungszentrum Jülich) for performing the SEM/EDS analysis.

CONFLICT OF INTEREST

The authors declare no conflict of interest.

ORCID

Markus Wolf https://orcid.org/0000-0003-2217-7563
Daniel Emil Mack https://orcid.org/0000-0002-0365-4582
Robert Vaßen https://orcid.org/0000-0002-9198-3991

REFERENCES

1. Koff B. Spanning the globe with jet propulsion. 21st Annual Meeting and Exhibit. Reston, VA: American Institute of Aeronautics and Astronautics; 2012. https://doi.org/10.2514/6.1991-2987
2. Miller RA. Thermal barrier coatings for aircraft engines: history and directions. J Therm Spray Technol. 1997;6:35–42.
3. Padture NP. Advanced structural ceramics in aerospace propulsion. Nat Mater. 2016;15:804–9.
4. Perepezko JH. Materials science. The hotter the engine, the better. Science. 2009;326:1068–9.
5. Bansal NP, Lamon J. Ceramic matrix composites: materials, modeling and technology. Hoboken, NJ: John Wiley & Sons, Inc; 2015. ISBN 978-1-118-23116-6.
6. Belmonte M. Advanced ceramic materials for high temperature applications. Adv Eng Mater. 2006;8:693–703.
7. Krenkel W, Berndt F. C/C–SiC composites for space applications and advanced friction systems. Mater Sci Eng A. 2005;412:177–81.
8. Carruth M, Baxter D, Oliveira F, Coley K. Hot-corrosion of silicon carbide in combustion gases at temperatures above the dew point of salts. J Eur Ceram Soc. 1998;18:2331–8.
9. Eaton HE, Linsey GD. Accelerated oxidation of SiC CMC's by water vapor and protection via environmental barrier coating approach. J Eur Ceram Soc. 2002;22:2741–7.
10. More KL, Tortorelli PF, Walker LR, Miriyala N, Price JR, Roode M, et al. High-temperature stability of SiC-based composites in high-water-vapor pressure environments. J Am Ceram Soc. 2003;86:1272–81.
11. Xu Y, Hu X, Xu F, Li K. Rare earth silicate environmental barrier coatings: present status and prospective. Ceram Int. 2017;43:5847–55.
12. Zhong X, Niu YR, Zhu T, Li H, Zheng XB, et al. Thermal shock resistance of Yb_2SiO_5/Si and $Yb_2Si_2O_7$/Si coatings deposited on C/SiC composites. J Am Ceram Soc. 2018;281:472–7.
13. Lee KN. Environmental barrier coatings for SiC f/SiC. In: Bansal NP, Lamon J, editors. Ceramic Matrix Composites. Hoboken, NJ: John Wiley & Sons, Inc; 2014: Vol. 80, p. 430–51. https://doi.org/10.1002/9781118832998.ch15.
14. Yang X, Zhao-hui C, Feng C. High-temperature protective coatings for C/SiC composites. J Asian Ceram Soc. 2014;2:305–9.
15. Lee KN, Eldridge JI, Robinson RC. Residual stresses and their effects on the durability of environmental barrier coatings for SiC ceramics. J Am Ceram Soc. 2005;88:3483–8.
16. Lee KN, Fox DS, Bansal NP. Rare earth silicate environmental barrier coatings for SiC/SiC composites and Si_3N_4 ceramics. J Eur Ceram Soc. 2005;25:1705–15.
17. Tian Z, Zheng L, Wang J, Yang J, Yang G, Wang J. Damage tolerance and extensive plastic deformation of β-$Yb_2Si_2O_7$ from room to high temperatures. J Am Ceram Soc. 2015;98:2843–51.
18. Zhu D. Advanced environmental barrier coatings for SiC/SiC ceramic matrix composite turbine components. In: Ohji T, Singh M, editors. Engineered Ceramics. Hoboken, NJ: John Wiley & Sons, Inc; 2016: Vol. 8, p. 6187–202. https://doi.org/10.1002/9781119100430.ch10
19. Sun Z, Zhou Y, Wang J, Li M. Thermal properties and thermal shock resistance of γ-$Y_2si_2O_7$. J Am Ceram Soc. 2008;91:2623–9.
20. van Roode M, Price JR, Stala C. Ceramic oxide coatings for the corrosion protection of silicon carbide. J Eng Gas Turbines Power. 1993;115:139–47.
21. Aparicio M, Durán A. Yttrium silicate coatings for oxidation protection of carbon-silicon carbide composites. J Am Ceram Soc. 2000;83:1351–5.
22. Chen WR, Zhao LR. Review – volcanic ash and its influence on aircraft engine components. Procedia Eng. 2015;99:795–803.
23. Dean J, Taltavull C, Clyne TW. Influence of the composition and viscosity of volcanic ashes on their adhesion within gas turbine aeroengines. Acta Mater. 2016;109:8–16.
24. Levi CG, Hutchinson JW, Vidal-Sétif M-H, Johnson CA. Environmental degradation of thermal-barrier coatings by molten deposits. MRS Bull. 2012;37:932–41.
25. Poerschke DL, Jackson RW, Levi CG. Silicate deposit degradation of engineered coatings in gas turbines: progress toward models and materials solutions. Annu Rev Mater Res. 2017;47:297–330.
26. Song W, Lavallée Y, Hess K-U, Kueppers U, Cimarelli C, Dingwell DB. Volcanic ash melting under conditions relevant to ash turbine interactions. Nat Commun. 2016;7:10795.
27. Grant KM, Krämer S, Seward GGE, Levi CG. Calcium-magnesium alumino-silicate interaction with yttrium monosilicate environmental barrier coatings. J Am Ceram Soc. 2010;93:3504–11.
28. Jang BK, Feng FJ, Suzuta K, Tanaka H, Matsushita Y, Lee KS, et al. Corrosion behavior of volcanic ash and calcium magnesium aluminosilicate on Yb_2SiO_5 environmental barrier coatings. J Ceram Soc Jpn. 2017;125:326–32. https://doi.org/10.2109/jcersj2.16211
29. Jiang F, Cheng L, Wang Y. Hot corrosion of RE_2SiO_5 with different cation substitution under calcium–magnesium–aluminosilicate attack. Ceram Int. 2017;43:9019–23.

30. Zhao H, Richards BT, Levi CG, Wadley HNG. Molten silicate reactions with plasma sprayed ytterbium silicate coatings. Surf Coat Technol. 2016;288:151–62.
31. Stolzenburg F, Johnson MT, Lee KN, Jacobson NS, Faber KT. The interaction of calcium–magnesium–aluminosilicate with ytterbium silicate environmental barrier materials. Surf Coat Technol. 2015;284:44–50.
32. Liu J, Zhang L, Liu Q, Cheng L, Wang Y. Calcium–magnesium–aluminosilicate corrosion behaviors of rare-earth disilicates at 1400°C. J Eur Ceram Soc. 2013;33:3419–28.
33. Turcer LR, Krause AR, Garces HF, Zhang L, Padture NP. Environmental-barrier coating ceramics for resistance against attack by molten calcia-magnesia-aluminosilicate (CMAS) glass: Part I, $YAlO_3$ and γ-$Y_2Si_2O_7$. J Eur Ceram Soc. 2018;38:3905–13.
34. Turcer LR, Krause AR, Garces HF, Zhang L, Padture NP. Environmental-barrier coating ceramics for resistance against attack by molten calcia-magnesia-aluminosilicate (CMAS) glass: Part II, β-$Yb_2Si_2O_7$ and β-$Sc_2Si_2O_7$. J Eur Ceram Soc. 2018;38:3914–24.
35. Stokes JL, Harder BJ, Wiesner VL, Wolfe DE. High-temperature thermochemical interactions of molten silicates with $Yb_2Si_2O_7$ and $Y_2Si_2O_7$ environmental barrier coating materials. J Eur Ceram Soc. 2019;39:5059–67.
36. Summers WD, Poerschke DL, Park D, Shaw JH, Zok FW, Levi CG. Roles of composition and temperature in silicate deposit-induced recession of yttrium disilicate. Acta Mater. 2018;160:34–46.
37. Summers WD, Poerschke DL, Taylor AA, Ericks AR, Levi CG, Zok FW. Reactions of molten silicate deposits with yttrium monosilicate. J Am Ceram Soc. 2020;103:2919–32.
38. Ahlborg NL, Zhu D. Calcium–magnesium aluminosilicate (CMAS) reactions and degradation mechanisms of advanced environmental barrier coatings. Surf Coat Technol. 2013;237:79–87.
39. Poerschke DL, Shaw JH, Verma N, Zok FW, Levi CG. Interaction of yttrium disilicate environmental barrier coatings with calcium-magnesium-iron alumino-silicate melts. Acta Mater. 2018;145:451–61.
40. Giordano D, Russell JK, Dingwell DB. Viscosity of magmatic liquids: a model. Earth Planet Sci Lett. 2008;271:123–34.
41. Zhou YC, Zhao C, Wang F, Sun YJ, Zheng LY, Wang XH. Theoretical prediction and experimental investigation on the thermal and mechanical properties of bulk β-$Yb_2Si_2O_7$. J Am Ceram Soc. 2013;96:3891–900.
42. Al Nasiri N, Patra N, Horlait D, Jayaseelan DD, Lee WE. Thermal properties of rare-earth monosilicates for EBC on Si-based ceramic composites. J Am Ceram Soc. 2016;99:589–96.
43. Dolan MD, Harlan B, White JS, Hall M, Misture ST, Bancheri SC, et al. Structures and anisotropic thermal expansion of the α, β, γ, and δ polymorphs of $Y_2Si_2O_7$. Powder Diffr. 2008;23:20–5.
44. Elkind A, Barsoum M, Kangutkar P. Thermal expansion of silicon carbide monofilaments and silicon carbide-borosilicate composites. J Am Ceram Soc. 1992;75:2871–3.
45. Reddy AA, Goel A, Tulyaganov DU, Kapoor S, Pradeesh K, Pascual MJ, et al. Study of calcium–magnesium–aluminum–silicate (CMAS) glass and glass-ceramic sealant for solid oxide fuel cells. J Power Sources. 2013;231:203–12.
46. Bansal NP, Choi SR. Properties of CMAS glass from desert sand. Ceram Int. 2015;41:3901–9.
47. Voron'ko YK, Sobol AA, Ushakov SN, Guochang J, Jinglin YL. Phase transformations and melt structure of calcium metasilicate. Inorg Mater. 2002;38:825–30.
48. Krause AR, Senturk BS, Garces HF, Dwivedi G, Ortiz AL, Sampath S, et al. $2ZrO_2{\cdot}Y_2O_3$ thermal barrier coatings resistant to degradation by molten CMAS: part I, optical basicity considerations and processing. J Am Ceram Soc. 2014;97:3943–9.
49. Duffy JA, Ingram MD. An interpretation of glass chemistry in terms of the optical basicity concept. J Non-Cryst Solids. 1976;21:373–410.
50. Duffy JA. Optical basicity analysis of glasses containing trivalent scandium, yttrium, gallium and indium. Phys Chem Glasses. 2005;46:500–4.
51. Duffy JA. Polarisability and polarising power of rare earth ions in glass: an optical basicity assessment. Phys Chem Glasses. 2005;46:1–6.
52. Nanba T, Miura Y, Sakida S. Consideration on the correlation between basicity of oxide glasses and O1s chemical Shift in XPS. J Ceram Soc Jpn. 2005;113:44–50.
53. Felsche J. The crystal chemistry of the rare-earth silicates. In: Dunitz JD, Hemmerich P, Ibers JA, Jørgensen CK, Neilands JB, Nyholm RS, Reinen D, Williams RJP, editors. Rare Earths. Berlin, Heidelberg: Springer Berlin Heidelberg; 1973: Vol. 13, p. 99–197. https://doi.org/10.1007/3-540-06125-8_3
54. Wiesner VL, Vempati UK, Bansal NP. High temperature viscosity of calcium-magnesium-aluminosilicate glass from synthetic sand. Scr Mater. 2016;124:189–92.
55. Becher PF, Ferber MK. Temperature-dependent viscosity of SiREAl-based glasses as a function of N:O and RE:Al ratios (RE = La, Gd, Y, and Lu). J Am Ceram Soc. 2004;87:1274–9.
56. Opila EJ, Smialek JL, Robinson RC, Fox DS, Jacobson NS. SiC recession caused by SiO_2 scale volatility under combustion conditions: II, thermodynamics and gaseous-diffusion model. J Am Ceram Soc. 1999;82:1826–34.
57. Krämer S, Yang J, Levi CG, Johnson CA. Thermochemical interaction of thermal barrier coatings with molten CaO-MgO-Al_2O_3-SiO_2 (CMAS) deposits. J Am Ceram Soc. 2006;89:3167–75.
58. Costa GCC, Jacobson NS. Mass spectrometric measurements of the silica activity in the Yb_2O_3–SiO_2 system and implications to assess the degradation of silicate-based coatings in combustion environments. J Eur Ceram Soc. 2015;35:4259–67.
59. Key TS, Presley KF, Hay RS, Boakye EE. Total thermal expansion coefficients of the yttrium silicate apatite phase $Y_{4.69}(SiO_4)_3O$. J Am Ceram Soc. 2014;97:28–31.
60. Pender DC, Padture NP, Giannakopoulos AE, Suresh S. Gradients in elastic modulus for improved contact-damage resistance. Part I: the silicon nitride–oxynitride glass system. Acta Mater. 2001;49:3255–62.
61. Jitcharoen J, Padture NP, Giannakopoulos AE, Suresh S. Hertzian-crack suppression in ceramics with elastic-modulus-graded surfaces. J Am Ceram Soc. 1998;81:2301–8.

How to cite this article: Wolf M, Mack DE, Guillon O, Vaßen R. Resistance of pure and mixed rare earth silicates against calcium-magnesium-aluminosilicate (CMAS): A comparative study. *J Am Ceram Soc*. 2020;103:7056–7071. https://doi.org/10.1111/jace.17328